CrossMark

O-Doped $Sb_{70}Se_{30}$ Phase-Change Materials for High Thermal Stability and Fast Speed

YUEMEI SUN,[1,5] YIFENG HU,[1,4,6] XIAOQIN ZHU,[1] HUA ZOU,[1]
YONGXING SUI,[1] JIANZHONG XUE,[1] LI YUAN,[1] JIANHAO ZHANG,[1]
LONG ZHENG,[1] DAN ZHANG,[2] and ZHITANG SONG[3]

1.—School of Mathematics and Physics, Jiangsu University of Technology, Changzhou 213001, People's Republic of China. 2.—School of Materials and Engineering, Jiangsu University of Technology, Changzhou 213001, People's Republic of China. 3.—State Key Laboratory of Functional Materials for Informatics, Shanghai Institute of Micro-System and Information Technology, Chinese Academy of Sciences, Shanghai 200050, People's Republic of China. 4.—State Key Lab of Silicon Materials, Zhejiang University, Hangzhou 310027, China. 5.—e-mail: sunym@jsut.edu.cn. 6.—e-mail: pcram@jsut.edu.cn

Oxygen doping was applied to improve the thermal stability of $Sb_{70}Se_{30}$ materials. Compared with $Sb_{70}Se_{30}$ film, the O-doped $Sb_{70}Se_{30}$ films exhibited higher crystallization temperature ($\sim$240°C), larger crystallization activation energy (4.99 eV) and better data retention (176.1°C for 10 years). O-doping also broadened the band gap and refined the grain size. A faster phase switching speed was obtained for O-doped $Sb_{70}Se_{30}$ materials. After O-doping, the phase change film had a smaller surface roughness (1.35 nm) than $Sb_{70}Se_{30}$.

Key words: $Sb_{70}Se_{30}$ material, oxygen-doping, thermal stability, fast speed

INTRODUCTION

In recent years, phase-change memory (PCM) has attracted more and more attention owing to its distinctive features such as low power consumption, cheap cost, fast speed and fabrication compatibility with the complementary metal–oxide–semiconductor (CMOS) process.[1–4] The data storage is realized by reversible phase transition between the 'reset' state (high-resistive amorphous state) and the 'set' state (low-resistive crystalline state) induced by electrical pulses. Due to the dramatic difference of resistivity between the two states, PCM devices may be used as practical high-performance memory elements.

The properties of PCM devices depend primarily on phase change materials.[5,6] Among many phase change chalcogenide materials, $Ge_2Sb_2Te_5$ (GST) has been widely studied.[7,8] Despite its remarkable properties, GST has been proved to have a quite low crystallization temperature (150°C),[9] poor 10-year

data retention (85°C),[10,11] relatively low crystallization speed (100 ns),[12] and large density change (6.5%).[13] In addition, in order to achieve higher storage density, the power consumption of PCM devices is another important factor that must be taken into account in practical applications.[14] Recently, benefiting from the growth-dominated crystallization mechanism of Sb, many Sb-rich alloys have been developed, such as Sb-Te, Al-Sb, Zn-Sb, and Ge-Sb.[15–18] However, Sb-rich phase change materials are also faced with a quite low crystallization temperature which reduces their thermal stability. Previous works have indicated that the thermal stability can be improved by doping. Oxygen doping is a common way to improve data retention by hindering crystallization and to lowering consumption by increasing resistivity.[19,20]

In this work, oxygen-doped $Sb_{70}Se_{30}$ phase-change thin films were fabricated by the radio-frequency (RF) sputtering method. The effect of oxygen doping on the thermal stability, crystallization characteristics, and optical transition of O-doped $Sb_{70}Se_{30}$ phase-change material was investigated in detail.

EXPERIMENTS

O-doped and undoped $Sb_{70}Se_{30}$ thin films were deposited on SiO_2/Si(100) substrates at room temperature by magnetron sputtering. The purity of $Sb_{70}Se_{30}$ target was 99.999% and thin film thickness was set to 50 nm through controlling the deposition time. The sputtering power of the $Sb_{70}Se_{30}$ target was set at 30 W. The pressures of the background and sputtering were 1×10^{-4} Pa and 3×10^{-1} Pa, respectively. O-doped thin film was obtained by mixing Ar and O_2 sputtering gas. The doping content of oxygen was controlled by adjusting the flow ratio of O_2/Ar, while the total gas flow was fixed at 30 sccm (standard cubic centimeter per minute at STP). The SbSe and SbSeOx (x = 1, 2, 3) films stand for undoped and O-doped $Sb_{70}Se_{30}$ films, respectively. The O concentrations of SbSeO1, SbSeO2 and SbSeO3 films, measured by x-ray photoelectron spectroscopy (XPS), were 9.3 at.%, 14.7 at.% and 19.2 at.%, respectively.

In situ temperature-dependent resistance (R–T) measurement was applied to investigate the amorphous-to-crystalline transition by using a TP 94 temperature controller (Linkam Scientific Instruments, Tadworth, Surrey, UK) under Ar atmosphere. The diffuse reflectivity spectra of the films were recorded by the NIR spectrophotometer (7100CRT; Xinmao, China). The phase structures of the films annealed at various temperatures were investigated by x-ray diffraction (XRD). The diffraction patterns were taken in the 2θ range from 20° to 60° using Cu Ka radiation with a scanning step of 0.01°/min. Picosecond laser technology was performed to measure the reflectivity change in real time during the phase transition process, using a picosecond frequency-doubled model-locked neodymium yttrium aluminum garnet laser operating at 532 nm wavelength with a pulse duration of 30 ps. The surface morphology of the films was observed by atomic force microscopy (AFM; FM-Nanoview 1000), which was carried out in the semi-contact mode.

RESULTS AND DISCUSSION

Figure 1 presents the resistances of pure $Sb_{70}Se_{30}$ and O-doped $Sb_{70}Se_{30}$ thin films as a function of temperature at a fixed heating rate of 10°C/min. The resistance of all the films was initially in a high-resistive amorphous state, and it decreased slowly along with temperature due to thermally assisted trap-limited conduction as a typical semiconductor. The temperature at which the amorphous resistance began to decrease abruptly was defined as the crystallization temperature, T_c. Figure 1 illustrates that the T_c of pure $Sb_{70}Se_{30}$ thin film was about 208°C. With increasing oxygen content in $Sb_{70}Se_{30}$ thin films, the T_c increased from about 225°C of the SbSeO1 thin film to about 240°C of the SbSeO3 thin film. Oxygen doping inhibits the crystallization and increases the crystallization temperature.

Generally, we can roughly consider that the higher T_c means better thermal stability. Therefore, oxygen doping enhances the thermal stability of SbSe thin films. Good thermal stability of the phase change materials is very significant in practical applications, because it can benefit the data retention and the reliability of the PCM devices. In order to confirm the crystallization state, the subsequent cooling process at the same rate was carried out. As shown in Fig. 1, the resistances were maintained in low values, indicating the occurrence of amorphous-to-crystalline phase change. Moreover, the resistances of the amorphous and crystallization states were increased after oxygen doping, which is helpful for reducing the RESET current by increasing the heating power according to the equation ($P = I^2R$). Therefore, compared with $Sb_{70}Se_{30}$ thin film, the PCM devices based on O-doped $Sb_{70}Se_{30}$ thin film will have lower power consumption.

The diffuse reflectivity spectra of undoped and O-doped $Sb_{70}Se_{30}$ thin films were measured by NIR spectrophotometry in the wavelength range from 400 to 2500 nm at room temperature. The band gap energy (E_g) could be determined by extrapolating the absorption edge onto the energy axis, as shown in Fig. 2, in which the conversion of the reflectivity to absorbance data was obtained by the Kubelka–Munk function (K–M)[21]:

$$K/S = (1 - R)^2/(2R) \tag{1}$$

where R is the reflectivity, K is the absorption coefficient, and S is the scattering coefficient. The band gap energy of SbSe, SbSeO1, SbSeO2 and SbSeO3 thin films were 0.74 eV, 0.90 eV, 0.99 eV, and 1.11 eV, respectively. With the increase of O concentration, the E_g of amorphous films was extended. In general, the carrier concentration inside the semiconductors is proportional to $\exp(-E_g/2k_bT)$, and the increase of the band gap
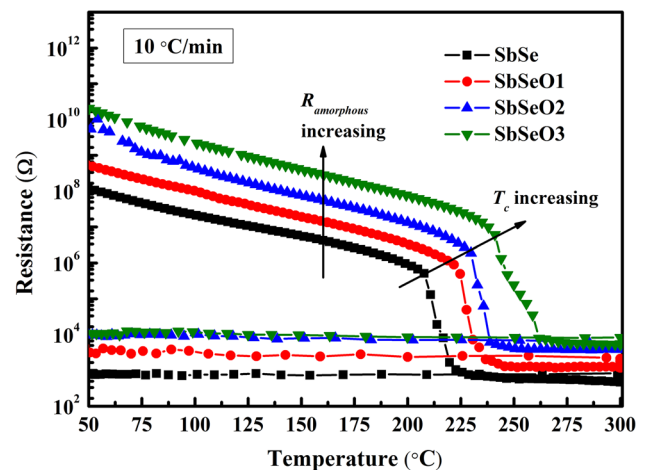

Fig. 1. R–T curves of undoped and O-doped $Sb_{70}Se_{30}$ thin films with a heating rate of 10°C/min.
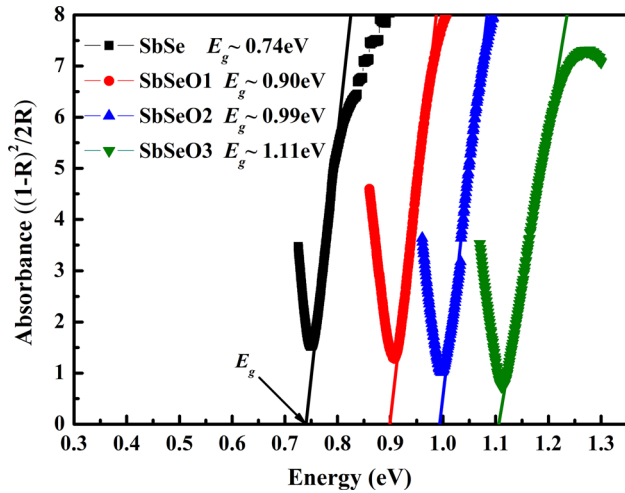
Fig. 2. The Kubelka–Munk function of undoped and O-doped amorphous Sb$_{70}$Se$_{30}$ thin films.

will result in the reduction of carriers, which make a major contribution to the increasing of film resistivity after more O-doping. The findings are in good agreement with the results from Fig. 1.

The data retention of phase change materials is an important parameter, especially with regard to the reliability of PCM. Isothermal change in time-dependent resistance at different temperatures was employed to evaluate the data retention of SbSeOx films. The failure time was defined as the time when the resistance reached half of its initial value at a specific isothermal temperature. Figure 3a–d shows the change of normalized resistance with time for the undoped and O-doped Sb$_{70}$Se$_{30}$ thin films. The typical inverse S-shaped growth curves can be seen for the isothermal crystallization, including incubation period, steady-state nucleation, growth, and coarsening.[22] A lower isothermal temperature will result in a longer failure time because it needs more time to accumulate the energy for the nucleation and grain growth. As shown in Fig. 3d, the failure time for SbSeO3 thin film was 28 s at the annealing temperature 240°C. Corresponding to the lower annealing temperatures, 235°C, 230°C, and 225°C, the failure time increased to 75 s, 277 s, and 867 s, respectively. Similar change trends could be obtained for other films.

The data retention was obtained by evaluating the failure time upon annealing temperature. The plot of logarithm failure time versus $1/k_b T$, shown in Fig. 3e, fits a linear Arrhenius relationship due to its thermal activation nature. In our case, the fitted straight line could be described by Eq. 2[23]

$$t = \tau_0 \exp(E_a/k_b T) \qquad (2)$$

where k_b, τ_0, t, E_a, and T are Boltzmann's constant, the pre-exponential factor depending on the material's properties, failure time, crystallization activation energy and absolute temperature of concern,
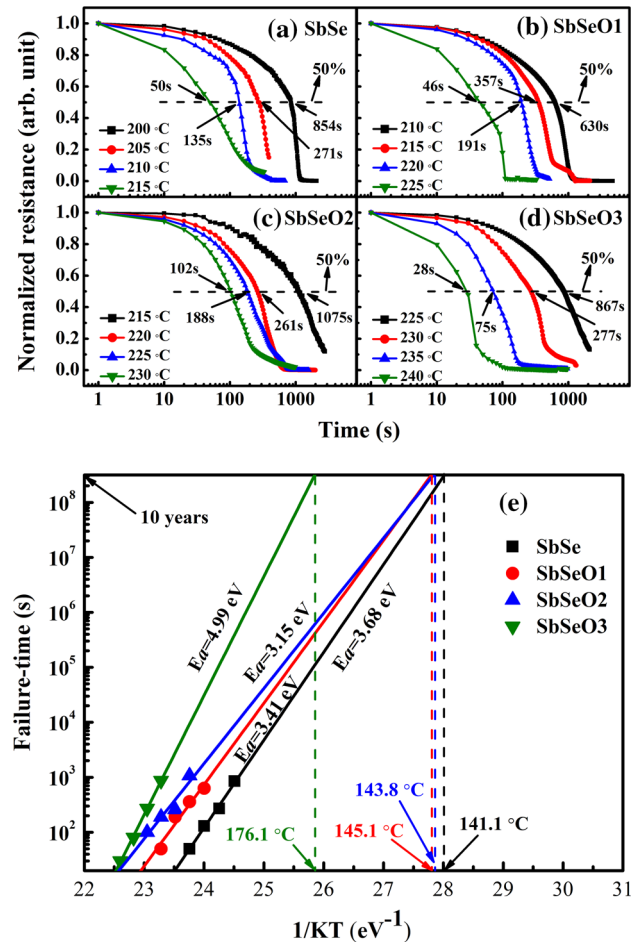

Fig. 3. (a–d) The change of normalized resistance with time for the undoped and O-doped Sb$_{70}$Se$_{30}$ thin films at isothermal annealing process. (e) Arrhenius plots of data retention showing extrapolated temperatures of 10-year data retention for the O-doped and undoped Sb$_{70}$Se$_{30}$ thin films.
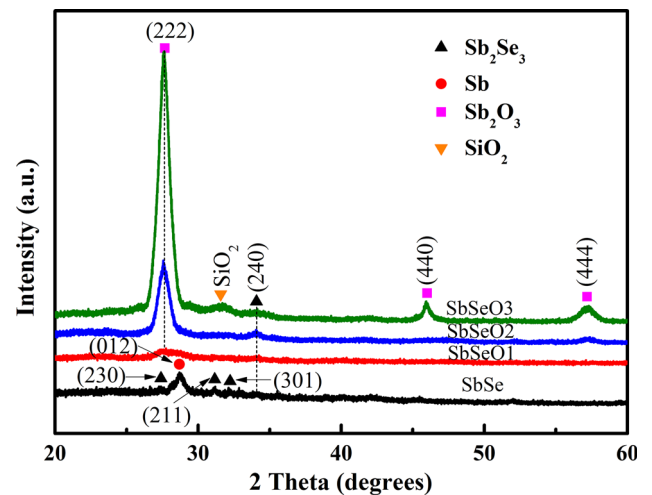

Fig. 4. XRD patterns of the SbSe and SbSeOx (x = 1, 2, 3) films annealed at 300°C for 10 min in Ar Atmosphere.

respectively. As shown in the extrapolated fit lines of Fig. 3e, the temperatures corresponding to a 10-year data retention $T_{10\text{-year}}$ were 145.1°C, 143.8°C, and 176.1°C for SbSeO1, SbSeO2, and SbSeO3, respectively. The undoped $Sb_{70}Se_{30}$ thin films could maintain a stable amorphous state for 10 years only when the environment temperature is 141.1°C. Compared with undoped $Sb_{70}Se_{30}$ thin films,
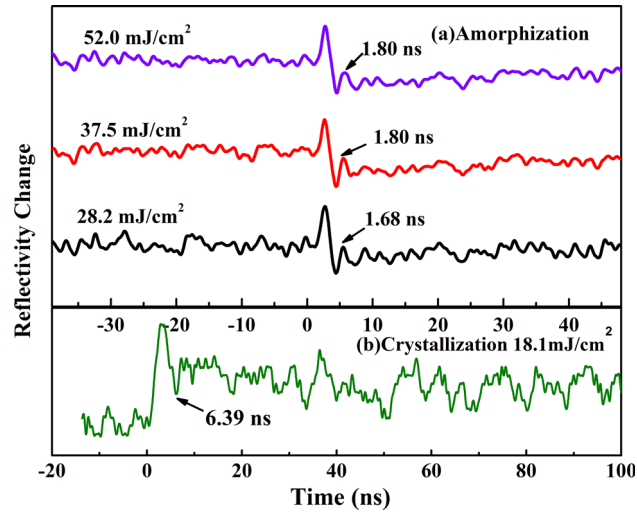

Fig. 5. Reversible reflectivity evolution of SbSeO2 thin films induced by consecutive picosecond laser pulses with different fluencies for (a) amorphization and (b) crystallizaton processes.

O-doped $Sb_{70}Se_{30}$ thin films possess better reliability of the resistance state at higher temperatures, which can satisfy the demands of data-storage applications at higher temperatures. The activation energy E_a for crystallization is a good estimate of the archival life stability of an amorphous phase change material. The E_a for SbSe, SbSeO1, SbSeO2, and SbSeO3 thin films, estimated by the slope of the fitted curves in Fig. 3e, were 3.68 eV, 3.41 eV, 3.15 eV, and 4.99 eV, respectively. In contrast, the E_a of GST is only 2.28 eV.[24] Thus, O-doped SbSe thin films had better data retention.

The crystalline structure of undoped and O-doped $Sb_{70}Se_{30}$ thin films was characterized by XRD. There were no diffraction peaks in any of the films at 25°C (not shown here), indicating that the as-deposited films are in amorphous states. Figure 4 presents the XRD patterns of SbSe and SbSeOx ($x = 1,2,3$) films annealed at 300°C for 10 min in Ar gas. The SiO_2 diffraction peak in the curve is caused by the $SiO_2/Si(100)$ substrate. For the SbSe films, the characteristic (230) (211), and (301) of the Sb_2Se_3 phase, as well as (012) of the Sb phase, appeared after annealing. These results demonstrate that the amorphous-to-crystalline transition occurred. The diffraction peak (012) of Sb disappeared after doping with oxygen. At the same time, the diffraction peaks (222) belonging to Sb_2O_3 appeared in the SbSeO1, SbSeO2 and SbSeO3 films, indicating new phases have formed after oxygen doping. That might be because the electronegativity
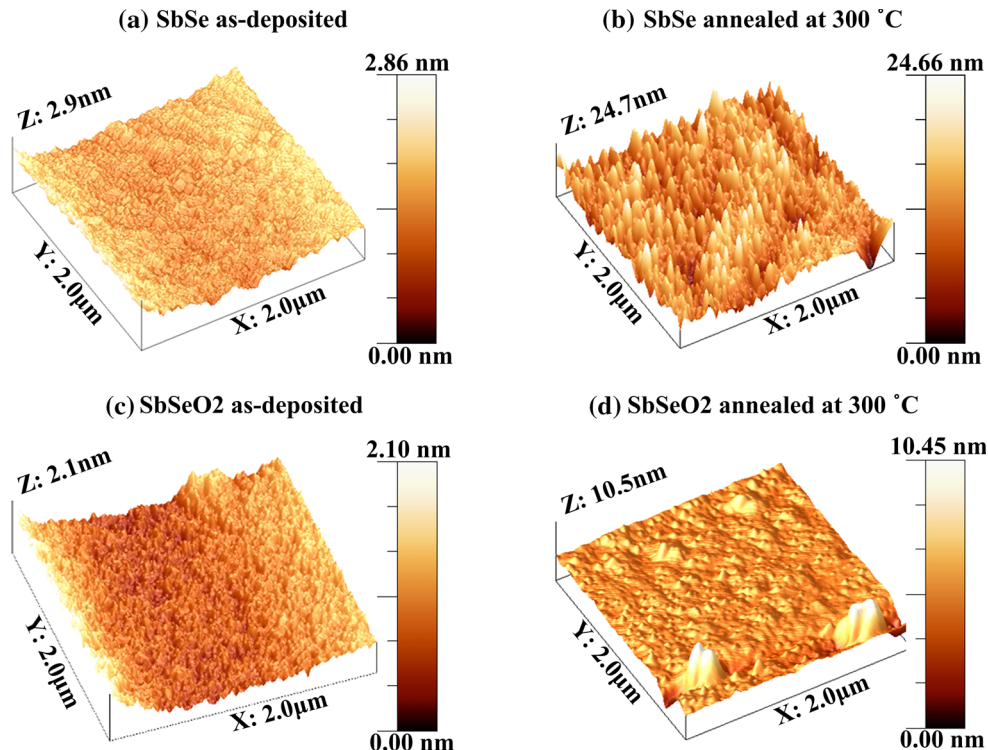

Fig. 6. AFM topographic images of (a) as-deposited SbSe, (b) annealed SbSe at 300°C, (c) as-deposited SbSeO2, and (d) annealed SbSeO2 at 300°C.

of the Sb and O elements is 1.8 and 3.5, respectively.[19] Some Sb atoms in the Sb–Sb bonds are replaced by oxygen atoms to form Sb-O oxides. The Sb-O oxides condense near grain boundaries and wrap around the crystal grains.[25] The atomic migration could be suppressed, resulting in smaller grain size and a larger number of grain boundaries.[4] The decreased grain size could produce more grain boundaries, which help to enhance the electron scattering, thus leading to a higher resistance.[26]

In the phase change, the changes of electrical resistivity are accompanied by optical reflectivity. In order to investigate the switching speed of the phase change materials, picosecond laser technology was applied. The reset operation needs more power and shorter time than the set one in the resistance switching process of PCM devices. Accordingly, more attention is paid to the reset power and the set speed.[27] That is to say, the power consumption and operation speed of PCM are mainly determined by the reset and set processes, respectively. In Fig. 5a, the reflectivity dropped, indicating the crystalline-to-amorphous state transition. Corresponding to different irradiation fluences of 28.2 mJ/cm^2, 37.5 mJ/cm^2 and 52.0 mJ/cm^2, the amorphization time were 1.68 ns, 1.80 ns and 1.80 ns, respectively. As shown in Fig. 5b, the crystallization time was 6.39 ns with the irradiation fluence of 18.1 mJ/cm^2. It has been reported that the crystallization time of GST is 23.1 ns.[28] Therefore, the SbSeO2 thin film has the faster phase switching speed.

Film surface roughness has a significant impact on device performance because the induced stress can affect the quality of the electrode–film interface during the phase change process.[29] The microstructure of the SbSe and SbSeO2 thin films before and after crystallization has been detected by AFM; the AFM images are shown in Fig. 6. The surfaces of the as-deposited SbSe and SbSeO2 thin films were very smooth, with the root-mean-square surface roughness 0.26 nm for SbSe and 0.25 nm for SbSeO2 thin films. After annealing at 300°C for 10 min, the roughness of the SbSe film increased to 2.51 nm due to the grain growth, while the roughness of the annealed SbSeO2 film increased slightly to 1.35 nm. This indicates that O-doping inhibits the grain growth, resulting in smaller grain size and better thermal stability.

CONCLUSION

In summary, O-doped Sb$_{70}$Se$_{30}$ materials were prepared and investigated for potential applications in PCM. O-doping improved the amorphous thermal stability of Sb$_{70}$Se$_{30}$ materials (SbSeO1: T_c 225°C, E_a 3.41 eV; SbSeO2: T_c 230°C, E_a 3.15 eV; SbSeO3: T_c 240°C, E_a 4.99 eV). The resistances of both amorphous and crystalline states for O-doped Sb$_{70}$Se$_{30}$ thin films increased with increasing O concentration, which will help to reduce the power consumption.

The $T_{10\text{-year}}$ of O-doped Sb$_{70}$Se$_{30}$ materials (SbSeO3: 176.1°C) was higher than that of GST. Moreover, the band-gap widths were extended after O-doping. The crystallization was restrained due to oxygen adding and a new Sb oxide phase formed. The crystallization time for SbSeO2 material induced by a picosecond laser pulse was much less than that of GST. In O-doped Sb$_{70}$Se$_{30}$ materials, the surface roughness became smaller (SbSeO2: 1.35 nm). These results demonstrated that the O-doped Sb$_{70}$Se$_{30}$ material is a promising candidate for good stability and low-power PCM applications.

REFERENCES

1. H. Volker, P. Jost, and M. Wuttig, *Adv. Funct. Mater.* 25, 6390 (2015).
2. Y.F. Hu, X.Q. Zhu, H. Zou, J.H. Zhang, L. Yuan, J.Z. Xue, Y.X. Sui, W.H. Wu, S.N. Song, and Z.T. Song, *Appl. Phys. Lett.* 108, 223103 (2016).
3. Z.M. Sun, J. Zhou, and R. Ahuja, *Phys. Rev. Lett.* 96, 055507 (2006).
4. Y.G. Lu, S.N. Song, X. Shen, Z.T. Song, G.X. Wang, and S.X. Dai, *Thin Solid Films* 589, 215 (2015).
5. D. Ielmini and A.L. Lacaita, *Mater. Today* 14, 600 (2011).
6. S.Y. Shin, J.M. Choil, J. Seo, H.W. Ahn, Y.G. Choi, B.L. Cheong, and S. Lee, *Sci Rep* 4, 7099 (2014).
7. R.E. Simpson, M. Krbal, P. Fons, A.V. Kolobov, J. Tominaga, T. Uruga, and H. Tanida, *Nano Lett.* 10, 414 (2010).
8. D. Loke, T.H. Lee, W.J. Wang, L.P. Shi, R. Zhao, Y.C. Yeo, T.C. Chong, and S.R. Elliott, *Science* 336, 1566 (2012).
9. M. Putero, T. Ouled-Khachroum, M.-V. Coulet, D. Deleruyelle, E. Ziegler, and C. Muller, *J. Appl. Crystallogr.* 44, 858 (2011).
10. Y.G. Lu, S.N. Song, Z.T. Song, F. Rao, L.C. Wu, M. Zhu, B. Liu, and D.N. Yao, *Appl. Phys. Lett.* 100, 193114 (2012).
11. C. Peng, L.C. Wu, F. Rao, Z.T. Song, P.X. Yang, H.J. Song, K. Ren, X.L. Zhou, M. Zhu, B. Liu, and J.H. Chu, *Appl. Phys. Lett.* 101, 122108 (2012).
12. G. Atwood, *Science* 321, 210 (2008).
13. W.K. Njoroge, H.W. Wöltgens, and M. Wuttig, *J. Vac. Sci. Technol.* 20, 230 (2002).
14. Y.G. Lu, S.N. Song, Y.F. Gong, Z.T. Song, F. Rao, L.C. Wu, B. Liu, and D.N. Yao, *Appl. Phys. Lett.* 99, 243111 (2011).
15. X.Q. Zhu, Y.F. Hu, J.Z. Xue, Y.X. Sui, W.H. Wu, L. Zheng, L. Yuan, S.N. Song, Z.T. Song, and S.P. Sun, *J. Mater. Sci.: Mater. El.* 25, 2943 (2014).
16. K.F. Kao, C.C. Chang, F.T. Chen, M.J. Tsai, and T.S. Chin, *Scr. Mater.* 63, 855 (2010).
17. T.J. Park, D.H. Kim, S.J. Park, S.M. Choi, K.J. Yoon, N.Y. Choi, N.Y. Lee, and B.G. Yu, *Jpn. J. Appl. Phys.* 46, L543 (2007).
18. S. Raoux, H.Y. Cheng, J.L. Jordan-Sweet, B. Munoz, and M. Hitzbleck, *Appl. Phys. Lett.* 94, 183114 (2009).
19. Hu, Y.F., Zhu, X.Q., Zou, H., Zheng, L., Song, S.N., Song, J.T.: *J. Alloy. Compd.* 696, 150 (2017). http://www.sciencedirect.com/science/journal/09258388/696/supp/C.

20. Y.F. Hu, M.C. Sun, S.N. Song, Z.T. Song, and J.W. Zhai, *J. Alloy. Compd.* 551, 551 (2013).
21. X.Q. Zhu, Y.F. Hu, L. Yuan, Y.X. Sui, J.Z. Xue, D.H. Shen, J.H. Zhang, S.N. Song, and Z.T. Song, *J. Electron. Mater.* 44, 3322 (2015).
22. Y.G. Lu, S.N. Song, X. Shen, Z.T. Song, L.C. Wu, G.X. Wang, and S.X. Dai, *Appl. Phys. A-Mater. Sci. Process.* 117, 1933 (2014).
23. Y.F. Hu, Z.F. He, J.W. Zhai, P.Z. Wu, T.S. Lai, S.N. Song, and Z.T. Song, *Appl. Phys. A* 121, 1125 (2015).
24. Y.F. Hu, H. Zou, J.H. Zhang, J.Z. Xue, Y.X. Sui, L. Yuan, W.H. Wu, X.Q. Zhu, S.N. Song, and Z.T. Song, *Appl. Phys. Lett.* 107, 263105 (2015).

25. C. Peng, L.C. Wu, F. Rao, Z.T. Song, X.L. Zhou, M. Zhu, B. Liu, D.N. Yao, S.L. Feng, P.X. Yang, and J.H. Chu, *Scripta Mater.* 65, 327 (2011).
26. W.H. Wu, Y.F. Hu, X.Q. Zhu, Y.X. Sui, L. Yuan, L. Zheng, H. Zou, Y.M. Sun, S.N. Song, and Z.T. Song, *J. Mater. Sci.: Mater. El.* 27, 2183 (2016).
27. Z.Y. Li, Y.F. Hu, T. Wen, J.W. Zhai, and T.S. Lai, *J. Appl. Phys.* 117, 135703 (2015).
28. W.H. Wu, Y.F. Hu, X.Q. Zhu, Y.X. Sui, J.Z. Xue, L. Yuan, S.N. Song, and Z.T. Song, *J. Mater. Sci.* 26, 9700 (2015).
29. T. Zhang, Z.T. Song, F. Wang, B. Liu, S.L. Feng, and B.M. Chen, *Appl. Phys. Lett.* 91, 221102 (2007).